



HAL
open science

Synthesis, NMR, vibrational spectroscopy, thermal and DFT studies of new DABCO hexafluorophosphate based ionic liquid

Boumediene Haddad, Silvia Brandán, Bekhaled Fetouhi, Mostefa Boumediene, Annalisa Paolone, Didier Villemin, Mustapha Rahmouni, Serge Bresson

► To cite this version:

Boumediene Haddad, Silvia Brandán, Bekhaled Fetouhi, Mostefa Boumediene, Annalisa Paolone, et al. Synthesis, NMR, vibrational spectroscopy, thermal and DFT studies of new DABCO hexafluorophosphate based ionic liquid. *Journal of Molecular Structure*, 2022, 1258, pp.132682. 10.1016/j.molstruc.2022.132682 . hal-03620215

HAL Id: hal-03620215

<https://hal.science/hal-03620215v1>

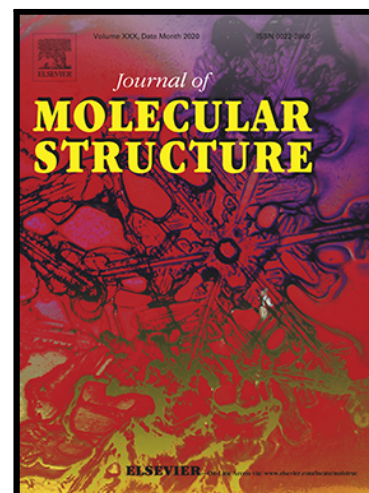
Submitted on 25 Mar 2022

HAL is a multi-disciplinary open access archive for the deposit and dissemination of scientific research documents, whether they are published or not. The documents may come from teaching and research institutions in France or abroad, or from public or private research centers.

L'archive ouverte pluridisciplinaire **HAL**, est destinée au dépôt et à la diffusion de documents scientifiques de niveau recherche, publiés ou non, émanant des établissements d'enseignement et de recherche français ou étrangers, des laboratoires publics ou privés.

Journal Pre-proof

Synthesis, NMR, vibrational spectroscopy, thermal and DFT studies of new DABCO hexafluorophosphate based ionic liquid



Boumediene Haddad , Silvia Antonia Brandán , Bekhaled Fetouhi ,
Mostefa Boumediene , Annalisa Paolone , Didier Villemin ,
Mustapha Rahmouni , Serge Bresson

PII: S0022-2860(22)00355-6
DOI: <https://doi.org/10.1016/j.molstruc.2022.132682>
Reference: MOLSTR 132682

To appear in: *Journal of Molecular Structure*

Received date: 18 August 2021
Revised date: 28 December 2021
Accepted date: 21 February 2022

Please cite this article as: Boumediene Haddad , Silvia Antonia Brandán , Bekhaled Fetouhi ,
Mostefa Boumediene , Annalisa Paolone , Didier Villemin , Mustapha Rahmouni , Serge Bresson ,
Synthesis, NMR, vibrational spectroscopy, thermal and DFT studies of new DABCO
hexafluorophosphate based ionic liquid, *Journal of Molecular Structure* (2022), doi:
<https://doi.org/10.1016/j.molstruc.2022.132682>

This is a PDF file of an article that has undergone enhancements after acceptance, such as the addition of a cover page and metadata, and formatting for readability, but it is not yet the definitive version of record. This version will undergo additional copyediting, typesetting and review before it is published in its final form, but we are providing this version to give early visibility of the article. Please note that, during the production process, errors may be discovered which could affect the content, and all legal disclaimers that apply to the journal pertain.

© 2022 Elsevier B.V. All rights reserved.

Synthesis, NMR, vibrational spectroscopy, thermal and DFT studies of new DABCO hexafluorophosphate based ionic liquid

Boumediene Haddad^{1,2,*}, Silvia Antonia Brandán³, Bekhaled Fetouhi^{4,5}, Mostefa Boumediene¹, Annalisa Paolone⁶, Didier Villemin², Mustapha Rahmouni⁵, Serge Bresson⁷.

¹ Chemistry Laboratory of Synthesis, Properties, and Applications (CLSPA-Saida), University of Saida, Algeria.

² LCMT, ENSICAEN, UMR 6507 CNRS, University of Caen, 6 bd Ml Juin, 14050 Caen, France

³ Cátedra de Química General, Instituto de Química Inorgánica, Facultad de Bioquímica. Química y Farmacia, Universidad Nacional de Tucumán, Ayacucho 471, (4000) San Miguel de Tucumán, Tucumán, Argentina.

⁴ Faculty of Natural and Life Sciences, University of Tiaret, BP78 Zaaroura Tiaret 14000, Algeria.

⁵ Synthesis and Catalysis Laboratory LSCT, Tiaret University, Tiaret, Algeria.

⁶ CNR-ISC, U.O.S. La Sapienza, Piazzale A. Moro 5, 00185 Roma, Italy

⁷ UP Transformations & Agro-Ressources, Institut Polytechnique UniLaSalle, SFR Condorcet 3417, BP 30313, F-60026 Beauvais, France.

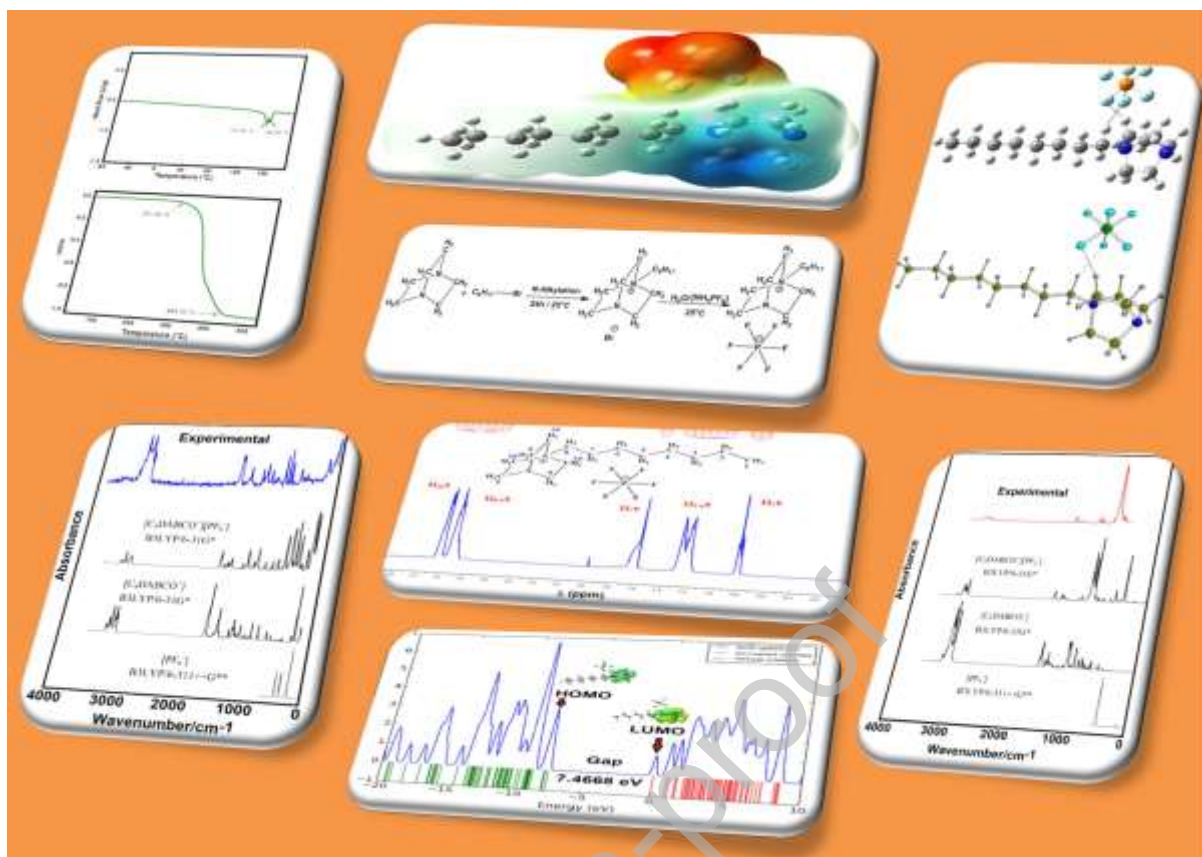
*Corresponding author: Tel: +213676802567

E-mail : haddadboumediene@yahoo.com (HADDAD Boumediene).

HIGHLIGHTS

- A new [C₈DABCO⁺][PF₆⁻] based ionic liquid
- The IL was characterized by using NMR and FTIR and Raman spectroscopies
- The thermal property of IL was investigated by means TGA and DTA measurements.
- B3LYP/6-31G* calculations support the high solvation energy value of IL
- DABCO structure plays a very important role in the properties of IL

Graphical abstract



ABSTRACT

In this paper, a new ionic liquid; $[\text{C}_8\text{DABCO}^+][\text{PF}_6^-]$ was prepared, its structure was well confirmed by ^1H , ^{13}C , ^{19}F and ^{31}P -NMR spectroscopies. Besides, thermal behavior has been discussed through TGA and DTA in the temperature range from $[-80$ to 200 °C] and $[25$ to 700 °C] respectively. Theoretical studies were performed by DFT method to investigate the structural, electronic and topological properties. B3LYP/6-31G* calculations support the high solvation energy value of IL in aqueous solution ($\Delta G_c = -122.9$ kJ/mol) and it probably explain the high dipole moment value, the volume expansion in this medium (7.3 Å³) and also because the cation-anion interactions still remain in solution. Seven interactions were predicted by AIM calculations but only two cation-anion interactions have short distances. NBO studies reveal that IL is more stable in solution probably due to its higher solvation energy. The DOS spectrum in aqueous solution shows clearly that the orbitals belonging to the atoms of cage-like DABCO structure participate in both HOMO and LUMO and, hence, will confirm that DABCO is engaged in halogen interactions, as suggested from NBO analyses. These studies show that DABCO structure participates in the properties of $[\text{C}_8\text{DABCO}^+][\text{PF}_6^-]$. Complete assignments of IR and Raman spectra were reported.

KEYWORDS: DABCO-ionic liquids; NMR; Raman/IR vibrational spectra; TGA /DTA thermal analysis; DFT calculations.

1. Introduction

Whatever material is used in a specific application, its properties depend on its structure and are strictly related to the nature of the intermolecular interactions between its constituents. Therefore, the comprehension of a relationship between the properties and the chemical architecture is essential for designing materials, in particular ionic liquids (ILs), with desirable properties.

Recently, a significant research effort has been focused on the synthesis and the physicochemical characterization of ionic liquids [1]. A special emphasis has been devoted to the study of their spectroscopy vibrational properties [2]. These new compounds can be useful in various areas and their important properties make them good candidates for multiple applications including catalytic reactions, engineering, inorganic chemistry, spectroscopy, electrochemistry and energetic material [3].

Compared to other ionic liquids, the synthesis and studies of DABCO ILs class are few, it was shown in last decade publications that a number of DABCO-based ionic liquids have characteristics that permit us to use them in many applications and especially for the catalytic reactions [4]

Elucidate the relation between the structure of ILs and their physicochemical properties it is a very difficult task. In this regards, detailed spectroscopic studies with the help of DFT calculations indicate that small changes in the structure of ILs (e.g. cation, anion or the alkyl group attached to the cation) give rise to a drastic change in their macroscopic properties and result in an important impact on physical properties such as melting points, viscosity and transport properties [5]. Consequently, the knowledge of their most stable chemical structure is required not only to understand the nature of ionic liquids and rationally expand their applications but also to assign the vibrational spectra.

IR and Raman spectroscopy have shown detailed information on the hydrogen-bonded interaction between coupled cation and anion in ionic liquids [6]; for example, by the combination of infrared/Raman spectroscopy studies with computational DFT methods. This way, the molecular structure, the intermolecular interactions and the vibrational spectra of $[\text{C}_8\text{DABCO}^+][\text{Br}^-]$ were recently investigated by us [7].

To the best of our knowledge and in contrast to the extensive studies on vibrational spectra of other ionic liquids, investigations of the vibrational properties of C_8DABCO are substantially fewer; this last theme is the subject of this paper. We will therefore systematically investigate the structural, thermal, electronic, topological and vibrational properties of

[C₈DABCO⁺][PF₆⁻] IL by using the experimental NMR, TGA/DTA, IR and FT-Raman spectra with the support of DFT calculations and the hybrid B3LYP/6-31G* method [8-9].

2. Materials and methods

All materials were of analytical grade and procured from Fluka. The precursors as DABCO (>99%), 1-bromooctane (98%), ammonium hexafluorophosphate (99.5 %), this includes solvents for the synthesis (ethyl acetate, diethyl ether and deionized H₂O).

2.1. Synthesis of [C₈DABCO⁺][PF₆⁻].

The detailed synthesis procedure for the first step was described in our previous paper [7]. In the second step, [C₈DABCO⁺][PF₆⁻] IL was subjected to anion exchange from bromide to hexafluorophosphate anion through a metathesis reaction according to the literature method [10]. The **Scheme 1** resume the synthetic procedure of [C₈DABCO⁺][PF₆⁻]. To elimination of possible water contamination before their use, [C₈DABCO⁺][PF₆⁻] was dried under vacuum (10⁻³ bar) on phosphorus pentoxide for 3 days. The determination of water was performed by coulometric Karl Fischer titration using a Metrohm 831 and was found below to 325 ppm. The NMR analysis (¹H, ¹³C, ¹⁹F, ³¹P-NMR) of [C₈DABCO⁺][PF₆⁻] IL is described in Section 3.2 and confirmed the structure of obtained [C₈DABCO⁺][PF₆⁻].

2.2.2. NMR measurements

The NMR analysis includes ¹H-NMR (500 MHz), ¹³C-NMR (125.75 MHz), ¹⁹F-NMR (470.62 MHz) and ³¹P-NMR (202.47 MHz) spectra were recorded by using Bruker DRX 500 MHz spectrometer. The chemical shifts (δ) are given in ppm and referenced to the internal solvent signal namely TMS, H₃PO₄ and CFCl₃, respectively. The coupling constants (J) are expressed in Hertz (Hz).

2.2.3. FT-Raman and FT-infrared measurements

The FT-Raman spectra of [C₈DABCO⁺][PF₆⁻] were acquired in the 45-4000 cm⁻¹ with a resolution of 1 cm⁻¹ and 128 scans at room temperature on a Vertex 70-RAM II Bruker FT-Raman spectrometer. Additionally; the FT-IR spectrum of [C₈DABCO⁺][PF₆⁻] in the solid state was recorded as KBr pellet between 4000 and 600 cm⁻¹ with a spectral resolution of 1 cm⁻¹ and 64 scans on a Bruker Vertex II-70RAM Spectrometer (Bruker Analytical, 7Slough, United Kingdom).

2.2.4. Thermal analysis

The thermal stability of $[\text{C}_8\text{DABCO}^+][\text{PF}_6^-]$ IL was examined using a Setaram Setsys Evolution 1200 TG System. The thermal analysis through DTA and TGA methods were collected from $[-80 \text{ to } 200 \text{ }^\circ\text{C}]$ and $[25 \text{ to } 700 \text{ }^\circ\text{C}]$ respectively at $5^\circ\text{C}/\text{min}$ in an argon flux of $60 \text{ ml}/\text{min}$ with the sample mass of $\sim 30 \text{ mg}$.

2.3. Computational details

The optimized cation and anion structures by using the B3LYP/6-31G* method from previous works reported by our research group were used to model the structure of $[\text{C}_8\text{DABCO}^+][\text{PF}_6^-]$ IL with the *GaussView* program [7,8, 9, 11]. After that, the optimizations of IL in the gas phase and in aqueous solution were carried out with the Gaussian 09 program [12]. As in similar works, the NBO and AIM 2000 programs have computed atomic charges, electrostatic potentials, bond orders, stabilization energies and topological properties [12-15] while reactivities and behaviours were performed with HOMO-LUMO calculations [7, 10-11]. Here, the *GaussView* program was employed as aid to perform the vibrational assignments of FTIR and FT-Raman spectra of $[\text{C}_8\text{DABCO}^+][\text{PF}_6^-]$ IL because the complete assignments for $[\text{C}_8\text{DABCO}^+]$ cation and $[\text{PF}_6^-]$ anion were already reported by separate with the scaled quantum mechanical force field (SQMFF) approach [7,11,16,17]. Better correlations between experimental and theoretical Raman spectra were obtained correcting activities at intensities, as suggested in the literature [18]. Finally, the ^1H -, ^{13}C -, ^{31}P - and ^{19}F -NMR chemical shifts were predicted in aqueous solution with the Gauge-Independent Atomic Orbital (GIAO) method and, later they were compared with the corresponding experimental ones [19]. In solution, the calculations were performed with the self-consistent reaction force (SCRF) method by using the integral equation formalism variant polarised continuum method (IEFPCM) and the solvation model [20-22]. The changes in the volume were calculated with the Moldraw program [23].

3. RESULTS AND DISCUSSION

3.1. Optimizations

The optimized structure of $[\text{C}_8\text{DABCO}^+][\text{PF}_6^-]$ IL in gas phase with C_1 symmetry by using the B3LYP/6-31G* method can be seen in **Figure 1** together with the atoms labelling and with the two closest interactions predicted between cation and anion which are: $\text{C7-H19}\cdots\text{F48}$ (2.072 \AA) and $\text{C20-H21}\cdots\text{F50}$ (2.156 \AA). In **Table 1** are shown calculated total energies (E), dipole moments (μ) and volumes of $[\text{C}_8\text{DABCO}^+][\text{PF}_6^-]$ IL in gas phase and

aqueous solution and its cation and anion in gas phase by using the B3LYP/6-31G* method. These results show that when the anion is incorporate to cation the expected volume of IL is $299.3 + 84.5 = 383.8 \text{ \AA}^3$, however, the calculated volume is lower (369.9 \AA^3) due to that the interactions between both species probably reduces it to 13.9 \AA^3 . In the same way, the total uncorrected energy between cation and anion by separate is $-660.2297 - 940.6432 = -1600.8729$ Hartrees, it is a lower value than the calculated (-1601.3896 Hartrees) due to the interactions between both species. Then, energies corrected by ZPVE in the three species decrease, comparing with corresponding uncorrected ones. Besides, when the cation interaction with the anion we observed that μ increases in the IL. Then, the effect of anion on μ of cation is very important in this IL because **Figure S1** shows that the path and direction of μ vector in the cation is different from the IL. This way, in the cation the direction of vector is from the C24 atom passing through the centre of the N23 atom, as it is observed in Figure S1 while the direction of the vector in the IL is perpendicular to the three rings and to the side chain. Hence, the anion produces modifications in the direction, orientation and magnitude of μ of cation. Besides, in aqueous solution the cation undergoes a strong expansion of volume (7.3 \AA^3) with an increase in the μ value from 14.39 D in gas phase to 20.86 D in solution. As a consequence of hydration, an increase in the distances of those two predicted interactions C7-H19...F48 (2.463 \AA) and C20-H21...F50 (2.436 \AA) are observed in solution. These interactions remain in solution probably due to its high corrected solvation energy because in aqueous solution its value is $\Delta G_c = -117.51 - 5.39 = -122.9 \text{ kJ/mol}$. The ΔG_c value is calculated with the E_{ZPVE} (solution – gas) and the value of non-electrostatic terms determined from PCM calculations by using the B3LYP/6-31G* method.

In **Table 2** only the predicted geometrical parameters related to N1 and N23 atoms of $[\text{C}_8\text{DABCO}^+][\text{PF}_6^-]$ ionic liquid in both media and to the bonds C7-H19 and C20-H21 lengths involved in the cation-anion interactions are compared with those reported for cation in gas phase by using the B3LYP/6-31G* method. The results show that the N-C distances of IL in gas phase practically are similar to cation while in the IL these distances are slightly different in both media. However, in solution the C7-H19 and C20-H21 distances present practically the same values while modifications in the H19-F48 and H21-F50 distances are observed, as was mentioned before. The values of IL are compared with the corresponding to cation by using the root means square deviation (RMSD) values. Higher variations are observed in the bond lengths ($1.405\text{-}1.404 \text{ \AA}$) as compared with the bond angles ($1.1\text{-}0.7^\circ$).

3.2. NMR Spectroscopic Characterization

In the order to obtain more information about the purity of $[C_8DABCO^+][PF_6^-]$ IL, the NMR analysis was investigated as preeminent technique for determining the structure of our investigated IL. The spectroscopic data are given below.

1H -NMR- $[C_8DABCO^+][PF_6^-]$, $(CDCl_3)$ δ_H (ppm) = 3.25–3.22 (m, 6H), 3.19 (m, 2H), 3.15–3.09 (m, 6H), 1.60–1.57 (m, 2H), 1.27–1.19 (m, 10H), 0.82–0.80 ppm (t, $J=10$ Hz, 3H).

^{13}C -NMR- $[C_8DABCO^+][PF_6^-]$, $(CDCl_3)$ δ_C (ppm) = 64.99, 52.65, 45.05, 31.57, 28.90, 26.08, 22.48, 21.80, 13.93.

^{19}F -NMR (DMSO- d_6) two signals at: -72.62, -71.14 (δ ppm: -71.88, doublet, $J_{FP}=711$ Hz).

^{31}P -NMR (DMSO- d_6) seven signals at: -133.76, -137.28, -140.77, -144.33, -147.85, -151.37, 154.94 (δ ppm: -144.33, septuplet, $J_{PF}=711$ Hz).

The 1H , ^{13}C , ^{19}F and ^{31}P -NMR for $[C_8DABCO^+][PF_6^-]$ IL are provided at (Figure 2a,b,c, d) respectively. These results confirm the structure of investigated $[C_8DABCO^+][PF_6^-]$ IL.

Compared to 1H -NMR spectra of $[C_8DABCO^+][Br^-]$ [6], the 1H -NMR spectra show more significant upfield shifts in the case of $[C_8DABCO^+][PF_6^-]$, this finding clearly indicates that the bromide anion has the ability to form a tighter interaction with $[C_8DABCO^+]$ cation than PF_6^- due to higher charge transfer in the case of the bromide anion. Furthermore, the chemical shifting towards upfield region values from bromide anion to PF_6^- , can be explained on basis of basicity nature and coordinating behaviour of anion. It is considered that PF_6^- anion acts as one of the least basic anions, larger and weaker coordinating anion. On the other hand, in ^{13}C -NMR spectrum of $[C_8DABCO^+][PF_6^-]$ (Figure 2b), nine signals were observed $[C_8DABCO^+][PF_6^-]$ between $\delta_C = 64.99$ and 13.93 ppm confirm the appropriate structure of $[C_8DABCO^+][PF_6^-]$. Moreover, the anionic exchange of bromide by hexafluorophosphate was demonstrated by the appearance of a doublet in the ^{19}F -NMR of $[C_8DABCO^+][PF_6^-]$ (Figure 2d) at -72.62 and -71.14 ppm from coupling between six equivalent fluorine nuclei ($spin=1/2$) and phosphorus nucleus ($spin=1/2$) with a coupling constant $J_{FP}=J_{PF}=711$ Hz. While, signal of P atom is appeared -144.33 ppm in ^{31}P -NMR spectrum (Figure 2c). On another side, in **Tables 3, 4** and **5** are compared the experimental 1H , ^{13}C and ^{19}F chemical shifts for IL dissolved in $CDCl_3$ with the corresponding theoretical in aqueous solution for cation and anion by using the B3LYP/6-31G* method and the RMSD values. Very good concordances were observed for the 1H nucleus (0.42–0.64 ppm) than the ^{13}C nucleus (5.44–11.84 ppm) and ^{19}F nucleus (6.61–4.37 ppm). Here, we have used CCl_3F as a reference to

obtain the signal of ^{19}F . The effect of incorporation of anion to cation is also observed in the predicted ^{13}C chemical shifts of IL which are high, as compared with the values of cation. However, the ^{19}F chemical shifts for IL present a better concordance (4.37 ppm) than the predicted for the anion (6.61 ppm). The high values observed in the H19 and H21 chemical shifts of IL in gas phase which change in solution, as compared to cation and to all H atoms, could explain the cation-anion interactions predicted for these two atoms. Besides, the highest chemical shift value observed in the C20 atom, that belong to C20-H21 bond of IL, could also be justified by the C20-H21...F50 interaction between cation and anion of IL. Hence, these studies clearly support the proposed theoretical structure of IL and the two interactions predicted in both media.

4.2. Atomic charges, bond orders and molecular electrostatic potentials

The presence of hydrophobic and hydrophilic sites is important structural requirement in a compound with potential biological activities because the existences of acceptors and donors groups justify its pharmacological properties. For these reasons, atomic charges and their distributions must be studied in this new derivative synthesized here. Therefore, the atomic natural population analysis (NPA), Merck-Kollman (MK) and Mulliken charges only for two N tertiary and quaternary atoms of $[\text{C}_8\text{DABCO}^+][\text{PF}_6^-]$ ionic liquid in both media by using the B3LYP/6-31G* method are compared in **Table S1** with the values corresponding to cation. Also, in the same table are presented the molecular electrostatic potentials (MEP) and bond orders, expressed as Wiberg indexes of IL and its cation in gas phase by using the same level of theory. The behaviours of these charges for both species in gas phase are presented in **Figure S2** while variations only for the IL in both media are shown in **Figure S3**. Here, the MK charges on N23 atoms of two species in gas phase evidence a very important because positive values are observed in the cation and IL while in the NPA charges are observed the same tendencies but on both atoms are evidenced negative values. On the other hand, different behaviours of Mulliken charges are revealed on both atoms different from MK and NPA charges where N23 atoms show most negative values. Other interesting observation is the similarity in three charges values on N23 atoms of two species while the N1 atoms show changes in the three charges. In solution, few variations are observed in the three charges on the two N atoms showing on N1 less negative values in this medium with exception of MK charge on N23 that is most negative than the other ones.

In relation to the molecular electrostatic potentials on both N atoms of IL in the two media, from **Table S1** and **Figure S4** it is observed most negative values on N1 of IL in gas phase

than N23 in solution. This result is in concordance with the positive MK charges evidenced on that atom in both media (Fig. S3). Besides, when the mapped MEP surface on the molecular surface of $[\text{C}_8\text{DABCO}^+][\text{PF}_6^-]$ IL in gas phase by using the B3LYP/6-31G* level of theory is represented in **Figure S5** we observed on $[\text{PF}_6^-]$ anion intense red colour, typical of nucleophilic places while on the $[\text{C}_8\text{DABCO}^+]$ cation positively charged it is observed blue colour characteristic of electrophilic sites. Green colours are observed on all atoms belong to the side chain where clearly these sites are inert.

Regarding the bond orders, expressed as Wiberg indexes of IL and its cation in gas phase by using the same level of theory from Table S1 and Figure S4, it is observed that the N23 atom of cation and IL present higher values than the N1. These values are calculated from Wiberg bond index and correspond to totals by atom but when Wiberg bond index matrix in the NAO basis are calculated it is observed that for the interaction C20-H21...F50 in gas phase the value decreases from 0.0214 in gas phase to 0.0148 in solution while the other C7-H19...F48 interaction decreases from 0.0242 in gas phase to 0.0129 in solution. These latter results are very important because these mean that both interactions remain in solution.

4.3. Stabilities by NBO and AIM studies

The studies of stabilities in ILs are very important because a weak interaction can disappear when change the medium from the gas phase to solution. Hence, two procedures were employed for $[\text{C}_8\text{DABCO}^+][\text{PF}_6^-]$ IL in order to analyze its stabilities in both media by using the same level of theory. First, the acceptors-donors interactions energies were calculated from Second Order Perturbation Theory Analysis of Fock Matrix in NBO Basis by using the NBO program [14] and, also the possible interactions have been studied with the Bader's theory of atoms in molecules in order to know the topological properties with the AIM 2000 program [15,16]. In the first case, the different interactions evidenced by NBO studies for cation and IL are observed in **Table S2**. The analyses show that cation presents only interactions from LP of N1 atom to three different antibonding C-C orbitals ($n \rightarrow \sigma^*$) while in the IL are observed, in addition to those observed for cation, two different types of interactions $\sigma \rightarrow \sigma^*$ and $\sigma^* \rightarrow \sigma^*$. These latter interactions occur from bonding σ_{P-F} and antibonding σ^*_{P-F} orbitals to antibonding σ^*_{P-F} orbitals and where both have energy values very high but in solution the contribution to the total energy is 12782.65 kJ/mol practically twice the value observed in gas phase (6621.29 kJ/mol). In the anion also was observed in gas phase by using the B3LYP/6-311++G** method six contributions $\sigma \rightarrow \sigma^*$ from bonding σ_{P-F} orbitals to antibonding σ^*_{P-F} orbitals each with the same values of 66.54 kJ/mol with a total

value of 399.27 kJ/mol. The high value of total energy observed for IL in aqueous solution could indicate that this IL is highly stable in this medium and probably a low reactivity is expected.

After that, the interactions in the IL have also been investigated calculating the topological properties with the AIM 2000 program [15,16]. Calculated properties in the bond critical points (BCPs) and ring critical points (RCPs) are: electron density, $\rho(r)$, the Laplacian values, $\nabla^2\rho(r)$, the eigenvalues (λ_1 , λ_2 , λ_3) of the Hessian matrix and, the $|\lambda_1/\lambda_3|$ ratio. **Table S3** shows analyses of the BCPs, RCPs and Cage critical points (CCP) of cation by using the B3LYP/6-31G* method in gas phase and only the BCPs of $[\text{C}_8\text{DABCO}^+][\text{PF}_6^-]$ ionic liquid are presented in the same table at the same level of theory. We observed that the cation presents only the H18...H25 interaction while only three F48, F49 and F50 atoms in the IL are involved in halogen interactions with H atoms of CH_2 groups linked to N23 atom and to the side chain. The above studies of MK charges in the IL have revealed that N23 is positively charged in both media and, for this reason, this DABCO moiety due to the cage-like structure is engaged in halogen interactions. In gas phase, are observed the seven P46-F48...H19, P46-F48...H21, P46-F48...H25, P46-F49...H15, P46-F49...H19, P46-F50...H15, P46-F50...H21 interactions where three RCPs generate a CCP (CC1). In **Figure S6** are observed positions of cage belonging to $[\text{C}_8\text{DABCO}^+]$ cation identifying the three rings with the atoms labelling [7]. The three RCPs of rings generate a CCP (CC1) while the other seven interactions generate seven new RCPNs which origin to CC2. These points are clearly observed for IL in both media in **Figure S7**. In solution, the P46-F48...H25 interaction disappear but appears the new C6-H17...H26 interaction and, hence, seven interactions are also observed in this medium. Here, it is necessary remember that when the requirements of: $\lambda_1/\lambda_3 < 1$ and $\nabla^2\rho(r) > 0$ hydrogen bonding or ionic interactions are observed. Analyzing all distances between two atoms in the interactions from Table S3 it is observed that in gas phase the two P46-F48...H19 and P46-F50...H21 interactions have low values while in solution the P46-F49...H19 and P46-F50...H21 interactions present lower distances together with the C6-H17...H26 interaction. These AIM results do not show differences for the ionic liquid in both media, while the NBO studies reveal that IL is more stable in solution.

4.4. Frontier Orbitals studies

The NBO calculations have suggested a low reactivity of IL in solution because it has a great stability in this media due to the high energetic interactions predicted in this medium. For

these reasons, the reactivities, stability kinetic and behaviours of $[\text{C}_8\text{DABCO}^+][\text{PF}_6^-]$ should be predicted by using the frontier orbitals, gap and descriptors as chemical potential (μ), electronegativity (χ), global hardness (η), global softness (S), global electrophilicity index (ω) and global nucleophilicity index (E) [7,10-11]. Thus, **Table S4** shows the results of those parameters for IL and its cation calculated in both media [6] by using the B3LYP/6-31G* method compared with reported for $[\text{Aliquat}^+][\text{NTf}_2^-]$ [24] and $[\text{Aliquat}^+][\text{Cl}^-]$ [25] ILs using the same level of calculation. Note that the $[\text{PF}_6^-]$ anion increase the gap values of $[\text{C}_8\text{DABCO}^+][\text{PF}_6^-]$ to 7.4368 eV in gas phase and 7.4668 eV in solution. However, the gap value in the $[\text{Aliquat}^+][\text{NTf}_2^-]$ is greater than $[\text{C}_8\text{DABCO}^+][\text{PF}_6^-]$ [24]. Then, increasing the gap value of IL implies that the reactivity decrease in both media. Now, to know the nature or characteristic of frontier orbitals in the studied IL and, especially in solution, the DOS spectrum was predicted at the same level of theory and the graphic can be seen in **Figure S8**. The figure shows clearly that orbitals belonging to the atoms of cage-like DABCO structure participate in both HOMO and LUMO and, hence, will confirm that DABCO is engaged in halogen interactions, as suggested from NBO analyses. Obviously, the DABCO structure plays a very important role in the properties of $[\text{C}_8\text{DABCO}^+][\text{PF}_6^-]$. Evaluating the descriptors we observed that the low reactivity of IL could be attributed to high global nucleophilicity indexes (E), as was also observed in the $[\text{C}_8\text{DABCO}^+]$ cation [6] and $[\text{Aliquat}^+][\text{NTf}_2^-]$ ionic liquid [24]. Another very important result observed here is the decreasing of global electrophilicity index (ω) of cation from 6.0990 eV to 1.9160-1.5595 eV in the IL. Such modifications are associated to anion.

4.5. Vibrational analyses

The optimized structure of $[\text{C}_8\text{DABCO}^+][\text{PF}_6^-]$ IL with the B3LYP/6-31G* method presents C_1 symmetry and has 52 atoms, hence, 150 normal vibration modes are expected. The experimental infrared and Raman spectra of IL in the solid phase are given in **Figures 3** and **4** which are compared with the predicted for IL and its cation and anion in the gas phase at different levels of theory. The effect of anion on cation is observed in the decreasing in the intensities of IR bands of cation and in the strong increase in the bands located in c.a.800 cm^{-1} attributed to P-F stretching modes of anion. An improvement between experimental and predicted Raman spectra of IL, cation and anion expressed activities is observed when they are corrected to intensities [17]. The scaled quantum mechanical force field (SQMFF) procedure and the Molvib program, the normal internal coordinates and transferable scaling factors were used for cation and anion of previous studies [7,11,17]. Here, the identifications

of all vibration modes of IL and its assignments were performed with the aid of *GaussView* program and considering a scaling factor of 0.95 [12]. Assignments for IL, cation and anion together with experimental and calculated wavenumbers are observed in **Table 6**. Here, in the lower wavenumbers region are evidenced the vibration modes corresponding to interactions cation-anion. Then, some assignments by regions are discussed by regions.

4.5.1. Assignments C-H groups.

4.5.1.1. 4000-2000 cm^{-1} region. Here, the scaling of calculated frequencies for IL generate resultant wavenumbers similar to predicted for the cation but the assignments change for $[\text{C}_8\text{DABCO}^+][\text{PF}_6^-]$ IL, as shown in Table 6. Thus, the group of bands in this region are easily assigned to antisymmetric and symmetric stretching modes of CH_2 and CH_3 groups of cation. As expected, the intense Raman band at 2974 cm^{-1} is assigned to symmetric stretching modes of these groups [7].

4.5.1.2. 2000-1000 cm^{-1} region. Here, also only are observed the vibration modes due to cation [7]. Hence, the assignments of CH_3 and CH_2 deformation, CH_2 wagging, CH_3 and CH_2 rocking modes are detailed in Table 6. Obviously, changes in the assignments of cation are expected in the ionic liquid at what time the anion is incorporate to cation. Thus, the strong infrared and Raman bands in $1069/1068 \text{ cm}^{-1}$ are assigned to C-C and C-N stretching modes. Both spectra show shoulders corresponding to most intense bands.

4.5.1.3. 1000-10 cm^{-1} region. This region is very important because the vibration modes of anion together with CH_3 and CH_2 twisting and C-C and C-N stretching and CCN, CCC skeletal modes are expected here [7,11]. The P-F stretching modes were assigned in the anion between 797 and 652 cm^{-1} while in this IL are these modes are predicted between 864 and 672 cm^{-1} [11]. Then, the very strong IR band at 833 cm^{-1} is clearly assigned to those vibration modes of anion. The P-F stretching mode predicted in the anion at 652 cm^{-1} in this IL when is scaled it is observed at 672 cm^{-1} . Other P-F stretching modes and the deformation modes predicted and assigned between 522 and 511 cm^{-1} in the anion, in this IL are predicted between 545 and 500 cm^{-1} [11]. In the anion, the wagging modes were predicted at 434 cm^{-1} while in the IL between 428 and 419 cm^{-1} . The rocking modes of PF_6^- anion were predicted at 285 cm^{-1} while in the ionic liquid at 281 , 272 and 268 cm^{-1} [11]. Obviously, these differences are attributed to interactions with the cation. The twisting mode of anion is predicted at 58 cm^{-1} while the Raman band at 239 cm^{-1} is assigned to twisting mode corresponding to CH_3 group, as predicted by scaling frequency.

The shoulder and the very strong Raman band observed in this region at 66 cm^{-1} is associated to a cation-anion interaction modes. Other skeletal modes are assigned as predicted by calculations and as observed in Table 6.

4.6. Thermal analysis

The thermal property of $[\text{C}_8\text{DABCO}^+][\text{PF}_6^-]$ was investigated by means of concomitant TGA/DTA measurements in order to obtain more information on its thermal behaviour. The experimental TGA/DTA are shown in **Figure 5**. Firstly, $[\text{C}_8\text{DABCO}^+][\text{PF}_6^-]$ shows two endothermic peaks around 151.66 and $156.50\text{ }^\circ\text{C}$, well within the thermal stability region, that could be attributed to a melting process. About TGA result, upon heating, we observed that the thermal decomposition occurs in the temperature range ≈ 271.55 to $444.10\text{ }^\circ\text{C}$, with a mass loss that reaches 87% at $444\text{ }^\circ\text{C}$ (see Figure 5). To the best of our knowledge, there are no other reports of the thermal stability or melting point of $[\text{C}_8\text{DABCO}^+][\text{PF}_6^-]$.

Conclusions

In this work, $[\text{C}_8\text{DABCO}^+][\text{PF}_6^-]$ was prepared and its structure characterized and confirmed by ^1H , ^{13}C , ^{31}P and ^{19}F -NMR spectroscopies. Its FT-infrared and FT-Raman spectra were measured and reported. Additionally, thermal stability of $[\text{C}_8\text{DABCO}^+][\text{PF}_6^-]$ and its decomposition process were discussed. The thermal behavior confirmed that $[\text{C}_8\text{DABCO}^+][\text{PF}_6^-]$ has shown good thermal stability. The experimental studies were accomplished with theoretical B3LYP/6-31G* calculations to optimize the structures in gas phase and aqueous solution and predict structural, electronic and topological properties. The IR, Raman and ^1H -, ^{13}C - and ^{19}F -NMR spectra were predicted and compared with the corresponding experimental ones. Good concordances were obtained in all cases. The high solvation energy value of IL in aqueous solution, $\Delta G_c = -122.9$ kJ/mol, could probably explain the high dipole moment value, the volume expansion in this medium (7.3 \AA^3) and also because the cation-anion interactions still remain in solution. Seven halogen interactions are predicted by AIM calculations but only two cation-anion interactions have short distances. AIM results do not show differences for the ionic liquid in both media while the NBO studies reveal that IL is more stable in solution probably due to its higher solvation energy. The DOS spectrum in aqueous solution shows clearly that the orbitals belonging to the atoms of cage-like DABCO structure participate in both HOMO and LUMO and, hence, will confirm that DABCO is engaged in halogen interactions, as suggested from NBO analyses. Obviously, the DABCO structure plays a very important role in the properties of $[\text{C}_8\text{DABCO}^+][\text{PF}_6^-]$. In addition, the bands observed in the IR and Raman spectra were completely assigned.

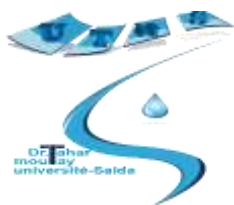
Acknowledgements

This research was carried out with grants from Ministry of Higher Education and Scientific Research (MESRS) of Algeria in PRFU project code: B00L01UN200120180002 and, from CIUNT Project N° 26/D608 (Consejo de Investigaciones, Universidad Nacional de Tucumán). The authors thank Prof. Tom Sundius for permission to use the MOLVIB program.

Supporting Information Available: Tables S1-S4 and Figures S1-S8.

Declaration of interests

The authors declare that they have no known competing financial interests or personal relationships that could have appeared to influence the work reported in this paper.

**DECLARATION OF INTEREST STATEMENT**

Boumediene Haddad: Writing - original draft; Conceptualization; Data curation; revision; Supervision.

Silvia Antonia Brandán: Validation; Visualization; Writing - original draft; revision; Writing - review & editing.

Bekhalel Fetouhi: Methodology; Data curation.

Mostefa Boumediene: Conceptualization; Data curation.

Annalisa Paolone: Conceptualization; Data curation.

Didier Villemin: Conceptualization; Project administration.

Mustapha Rahmouni: Conceptualization; Data curation.

Serge Bresson: Methodology; Resources.

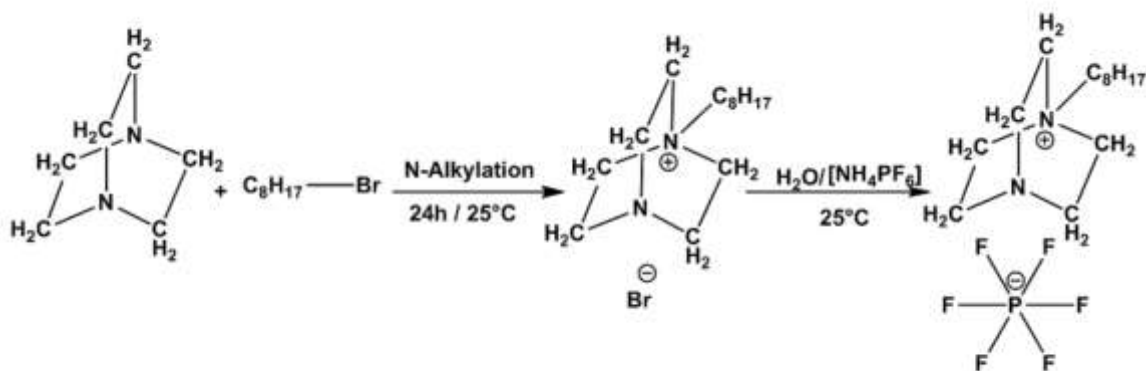
References

- [1] C. Ferrara, V. Dall'Asta, V. Berbenni, E. Quartarone, & P. Mustarelli, Physicochemical characterization of AlCl₃-1-Ethyl-3-methylimidazolium chloride ionic liquid electrolytes for aluminum rechargeable batteries. *J. Phys. Chem. C*. 121(48) (2017) 26607-26614.
<https://doi.org/10.1021/acs.jpcc.7b07562>
- [2] M. Drai, A. Mostefai, A. Paolone, B. Haddad, E. Belarbi, D. Villemin, ... & M. Rahmouni, Synthesis, experimental and theoretical vibrational studies of 1-methyl and 1, 2-

- dimethyl, 3-propyl imidazolium bis (trifluoromethanesulfonyl) imide. *J Chem Sci*, 129(6) (2017) 707-719. <https://doi.org/10.1007/s12039-017-1282-6>
- [3] S. K. Singh & A. W. Savoy, Ionic liquids synthesis and applications: An overview. *J. Mol. Liq.* 297 (2020) 112038. <https://doi.org/10.1016/j.molliq.2019.112038>
- [4] N. Jamasbi, M. Irankhah-Khanghah, F. Shirini, H. Tajik & M. S. N. Langarudi, DABCO-based ionic liquids: introduction of two metal-free catalysts for one-pot synthesis of 1, 2, 4-triazolo [4, 3-a] pyrimidines and pyrido [2, 3-d] pyrimidines. *NJC* .42(11) (2018) 9016-9027. <https://doi.org/10.1039/C8NJ01455H>
- [5] M. A. Varfolomeev, A. A. Khachatryan, B. S. Akhmadeev & B. N. Solomonov, Thermodynamics of hydrogen bonding and van der Waals interactions of organic solutes in solutions of imidazolium based ionic liquids: “Structure-property” relationships. *Thermochim. Acta.* 633(2016) 12-23. <https://doi.org/10.1016/j.tca.2016.03.036>
- [6] B. A. Omidvar, S. F. Tayyari, M. Vakili, & A. R. Nekoei, Vibrational spectra, normal coordinate analysis, and hydrogen bond investigation of pyridinium perchlorate. *Spectrochim. Acta A Mol. Biomol. Spectrosc.* 191 (2018)558-565. <https://doi.org/10.1016/j.saa.2017.10.067>
- [7] B. Fetouhi, B. Haddad, S. A. Brandán, A. Paolone, D. Villemin, M. Boumediene,... & S. Bresson, Synthesis, molecular structure, and properties of DABCO bromide based ionic liquid combining spectroscopic studies with DFT calculations. *J. Mol. Struct.* 1233 (2021) 130102. <https://doi.org/10.1016/j.molstruc.2021.130102>
- [8] A.D. Becke, Density-functional exchange-energy approximation with correct asymptotic behavior, *Phys. Rev. A*38 (1988) 3098-3100. <https://doi.org/10.1103/PhysRevA.38.3098>
- [9] C. Lee, W. Yang, R.G. Parr, Development of the Colle-Salvetti correlation-energy formula into a functional of the electron density, *Phys. Rev. B*37 (1988) 785-789. <https://doi.org/10.1103/PhysRevB.37.785>
- [10] M. Boumediene, B. Haddad, A. Paolone, M. A. Assenine, D. Villemin, M. Rahmouni & S. Bresson, Synthesis, conformational studies, vibrational spectra and thermal properties, of new 1, 4-(phenylenebis (methylene) bis (methyl-imidazolium) ionic liquids, *J. Mol. Struct.* 1220 (2020) 128731. <https://doi.org/10.1016/j.molstruc.2020.128731>
- [11] B. Haddad, S. A. Brandán, M. A. Assenine, A. Paolone, D. Villemin, & S. Bresson, Bidentate cation-anion coordination in the ionic liquid 1-ethyl-3-methylimidazolium hexafluorophosphate supported by vibrational spectra and NBO, AIM and SQMFF calculations, *J. Mol. Struct* 1212 (2020) 128104. <https://doi.org/10.1016/j.molstruc.2020.128104>
- [12] J. Frisch, G. W. Trucks, H. B. Schlegel, G. E. Scuseria, et al., Gaussian 09, Revision A.02, M. Gaussian, Inc., Wallingford CT, 2009.
- [13] A.B. Nielsen, A.J. Holder, Gauss View 5.0, User's Reference, GAUSSIAN Inc., Pittsburgh, PA, 2008.
- [14] E.D. Glendening, J.K. Badenhoop, A. D. Reed, J. E. Carpenter, F. Weinhold, NBO 3.1; Theoretical Chemistry Institute, University of Wisconsin; Madison, WI, 1996.
- [15] R.F.W. Bader, Atoms in Molecules, A Quantum Theory, Oxford University Press, Oxford, 1990, ISBN: 0198558651. https://www.schulz.chemie.uni-rostock.de/storages/uni-rostock/Alle_MNF/Chemie_Schulz/Computerchemie_3/advanced/aim_theory.pdf

- [16] F. Biegler-König, J. Schönbohm, D. Bayles. AIM2000; A Program to Analyze and Visualize Atoms in Molecules, *J. Comput. Chem.* 22 (2001) 545.
[https://doi.org/10.1002/1096-987X\(20010415\)22:5<545::AID-JCC1027>3.0.CO;2-Y](https://doi.org/10.1002/1096-987X(20010415)22:5<545::AID-JCC1027>3.0.CO;2-Y)
- [17] P. Pulay, G. Fogarasi, G. Pongor, J.E. Boggs, A. Vargha, Combination of theoretical *ab initio* and experimental information to obtain reliable harmonic force constants. Scaled quantum mechanical (QM) force fields for glyoxal, acrolein, butadiene, formaldehyde, and ethylene. *J. Am. Chem. Soc.* 105 (1983) 7073.
<https://doi.org/10.1021/ja00362a005>
- [18] G. Keresztury, S. Holly, G. Besenyi, J. Varga, A.Y. Wang, J.R. Durig, Vibrational spectra of monothiocarbamates-II. IR and Raman spectra, vibrational assignment, conformational analysis and **ab initio** calculations of **S**-methyl-**N,N**-dimethylthiocarbamate *Spectrochim. Acta.* 49A (1993) 2007-2026.
[https://doi.org/10.1016/S0584-8539\(09\)91012-1](https://doi.org/10.1016/S0584-8539(09)91012-1)
- [19] R. Ditchfield, Self-consistent perturbation theory of diamagnetism. I. A gage-invariant LCAO (linear combination of atomic orbitals) method for NMR chemical shifts, *Mol. Phys.* 27 (1974) 714–722. <https://doi.org/10.1080/00268977400100711>
- [20] S. Miertus, E. Scrocco, J. Tomasi, Electrostatic interaction of a solute with a continuum. *Chem. Phys.* 55 (1981) 117–129. [https://doi.org/10.1016/0301-0104\(81\)85090-2](https://doi.org/10.1016/0301-0104(81)85090-2)
- [21] J. Tomasi, J. Persico, Molecular Interactions in Solution: An Overview of Methods Based on Continuous Distributions of the Solvent, *Chem. Rev.* 94 (1994) 2027-2094.
<https://doi.org/10.1021/cr00031a013>
- [22] A.V. Marenich, C.J. Cramer, D.G. Truhlar, Universal solvation model based on solute electron density and a continuum model of the solvent defined by the bulk dielectric constant and atomic surface tensions, *J. Phys. Chem. B* 113 (2009) 6378-6396.
<https://doi.org/10.1021/jp810292n>
- [23] P. Ugliengo, MOLDRAW Program, University of Torino, Dipartimento Chimica IFM, Torino, Italy, 1998.
- [24] M. A. Assenine, B. Haddad, A. Paolone, S. A. Brandán, M. Goussein, D. Villemin, ... & S. Bresson, Synthesis, thermal properties, vibrational spectra and computational studies of Trioctylammonium bis (trifluoromethylsulfonyl) imide ionic liquid. *J. Mol. Struct.* 1232 (2021) 130085. <https://doi.org/10.1016/j.molstruc.2021.130085>
- [25] M. A. Assenine, B. Haddad, A. Paolone, S. A. Brandán, D. Villemin, M. Boumediene, ... & S. Bresson, Experimental and DFT studies on structure, spectroscopic and thermal properties of N-Methyl-N, N, N-trioctylammonium chloride ionic liquid. *J. Mol. Struct.* 1230 (2021) 129625. <https://doi.org/10.1016/j.molstruc.2020.129625>

Caption Figures



Scheme 1. General synthesis of $[C_8DABCO^+][PF_6^-]$.

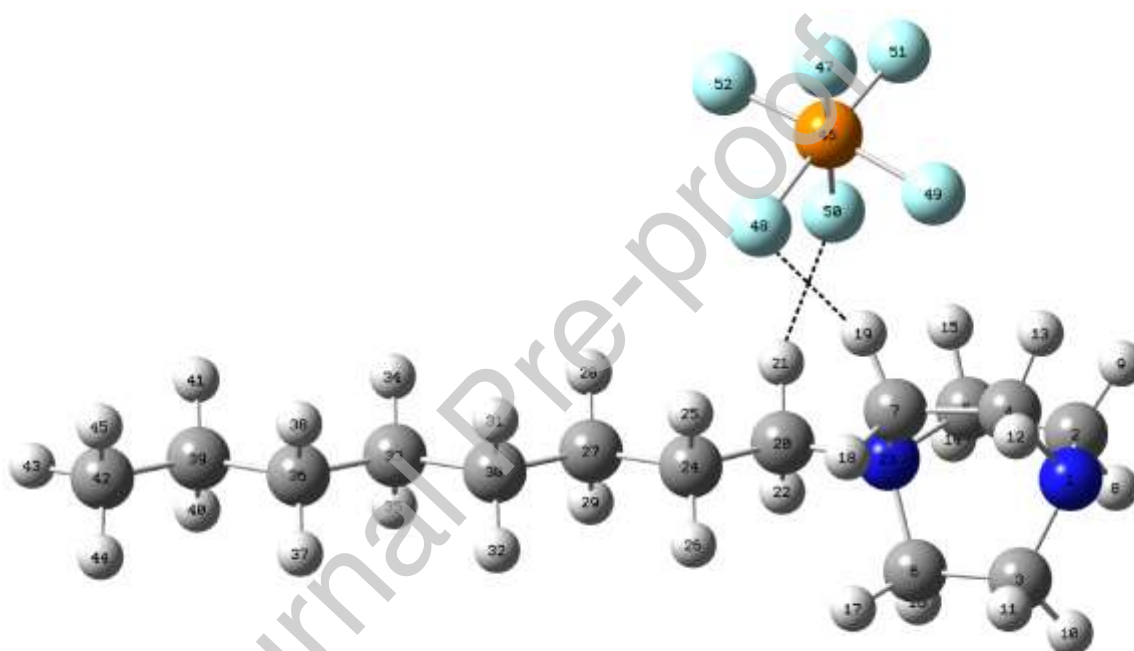
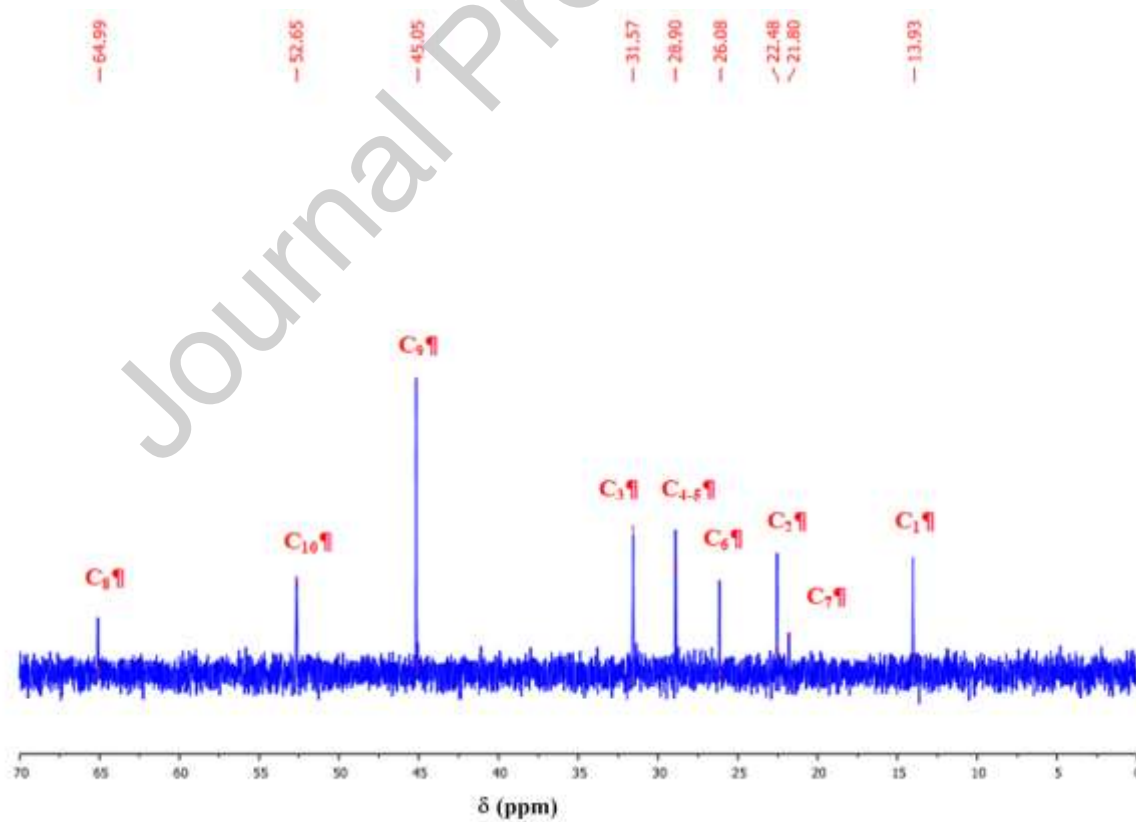
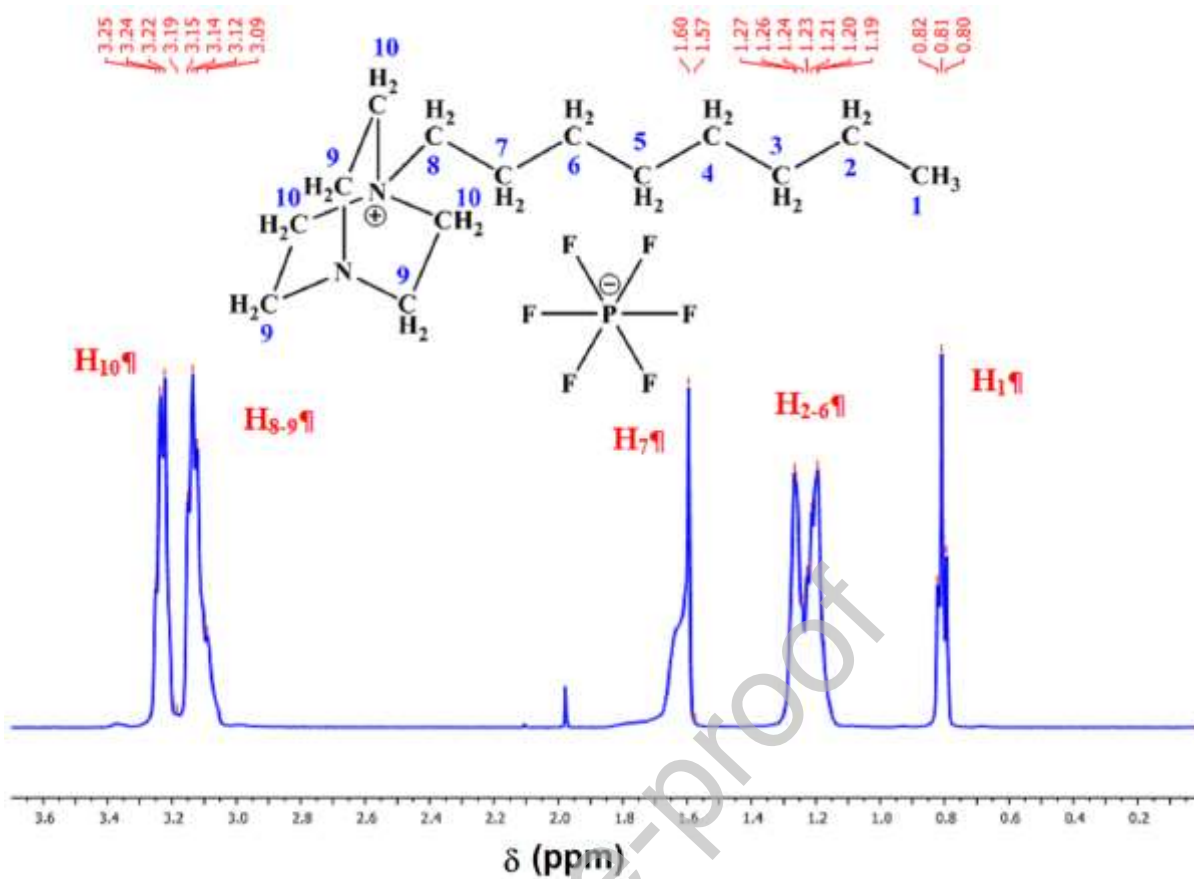


Figure 1. Optimized structure of $[C_8DABCO^+][PF_6^-]$ IL in gas phase by using the B3LYP/6-31G* method and atoms labelling.



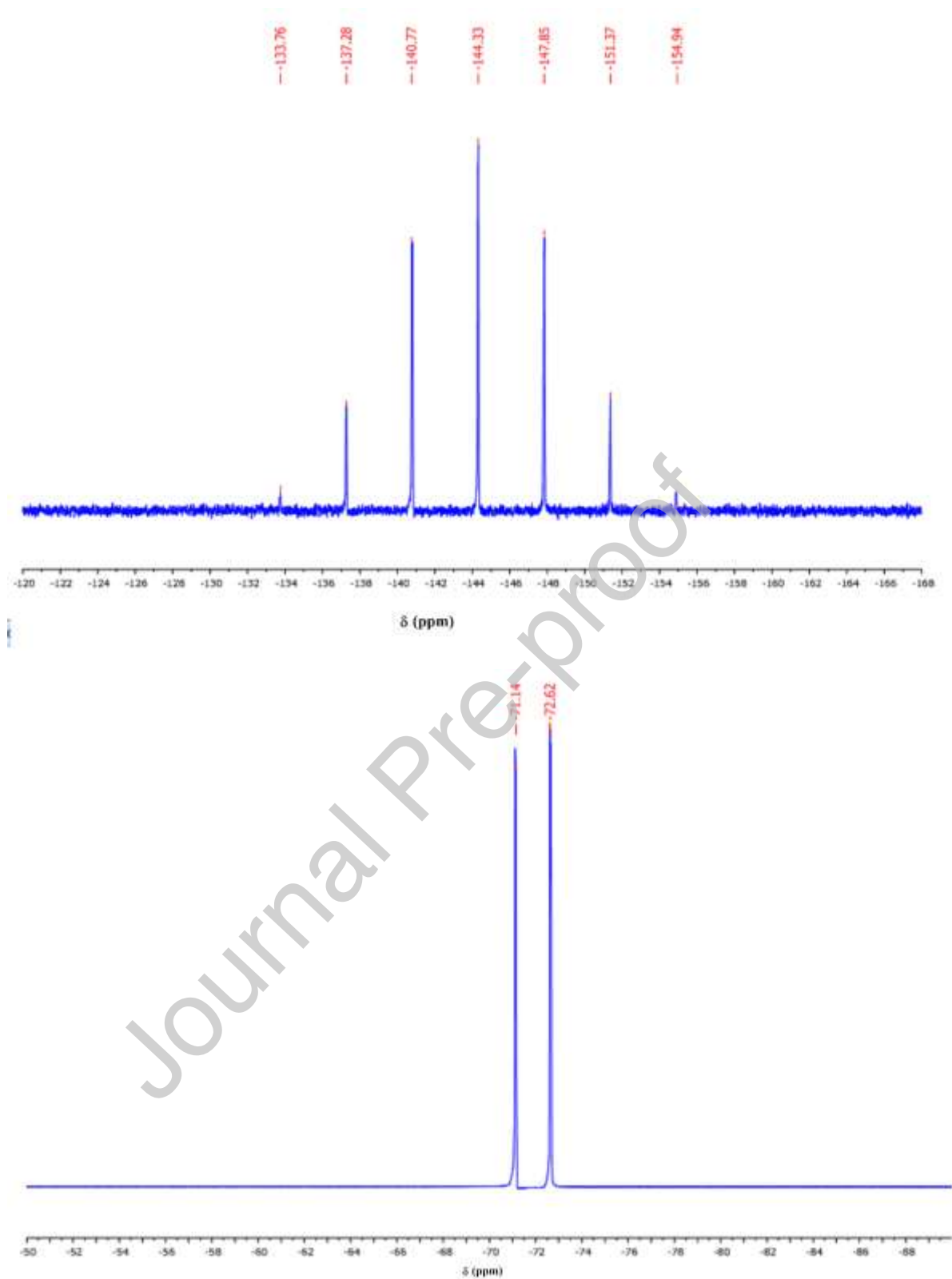


Figure 2. NMR spectra of [C₈DABCO⁺][PF₆⁻] IL in CDCl₃ solution over the scan range 0 to 10 δ ppm for ¹H-NMR (a), from 0 to 70 δ ppm for ¹³C-NMR (b), from -120 to -168 δ ppm for ³¹P-NMR (c) and -50 to -90 δ ppm for ¹⁹F-NMR (d).

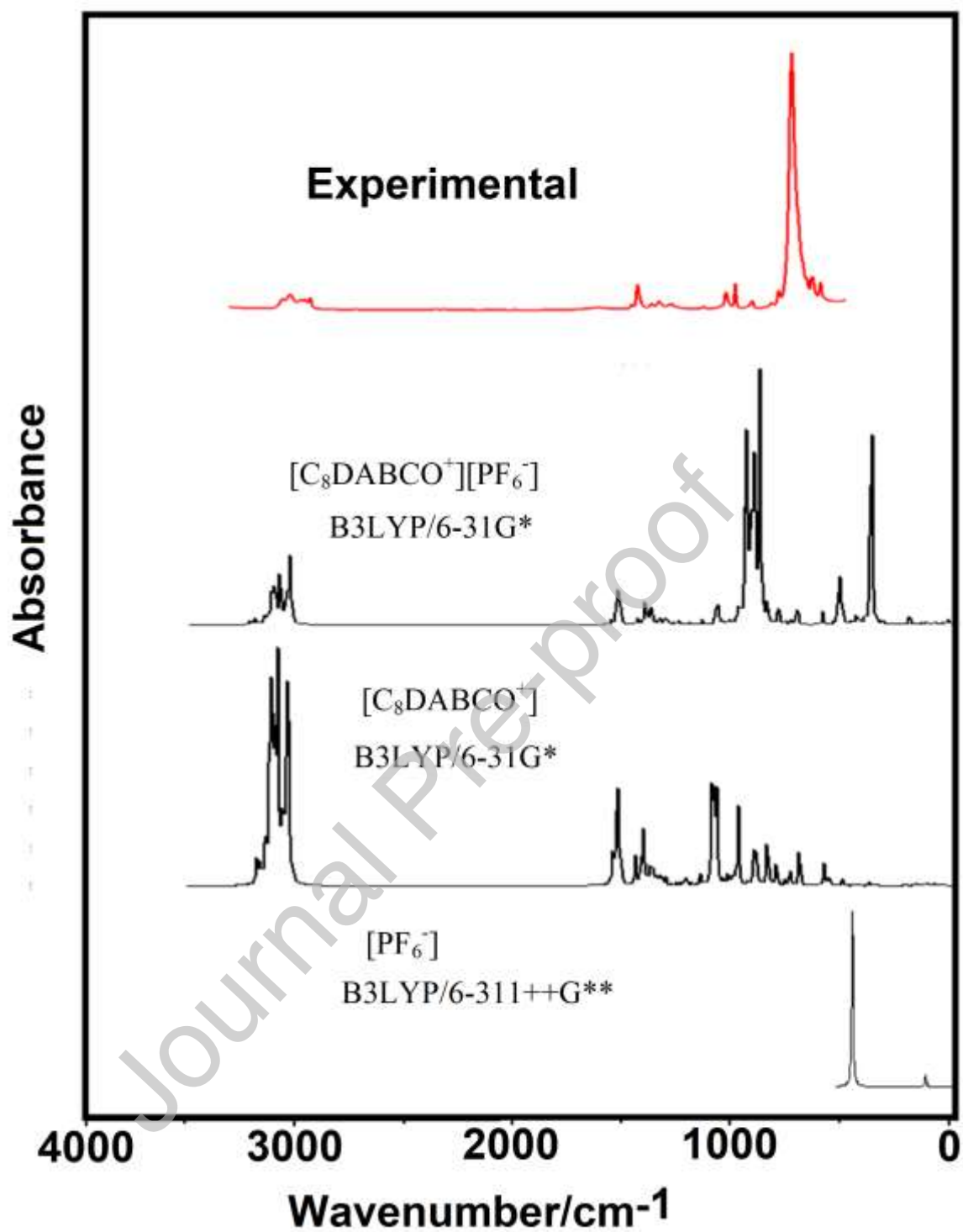


Figure 3. Experimental FT-IR of [C₈DABCO⁺][PF₆⁻] IL compared with the corresponding predicted for the cation and anion by using the B3LYP/6-31G* method.

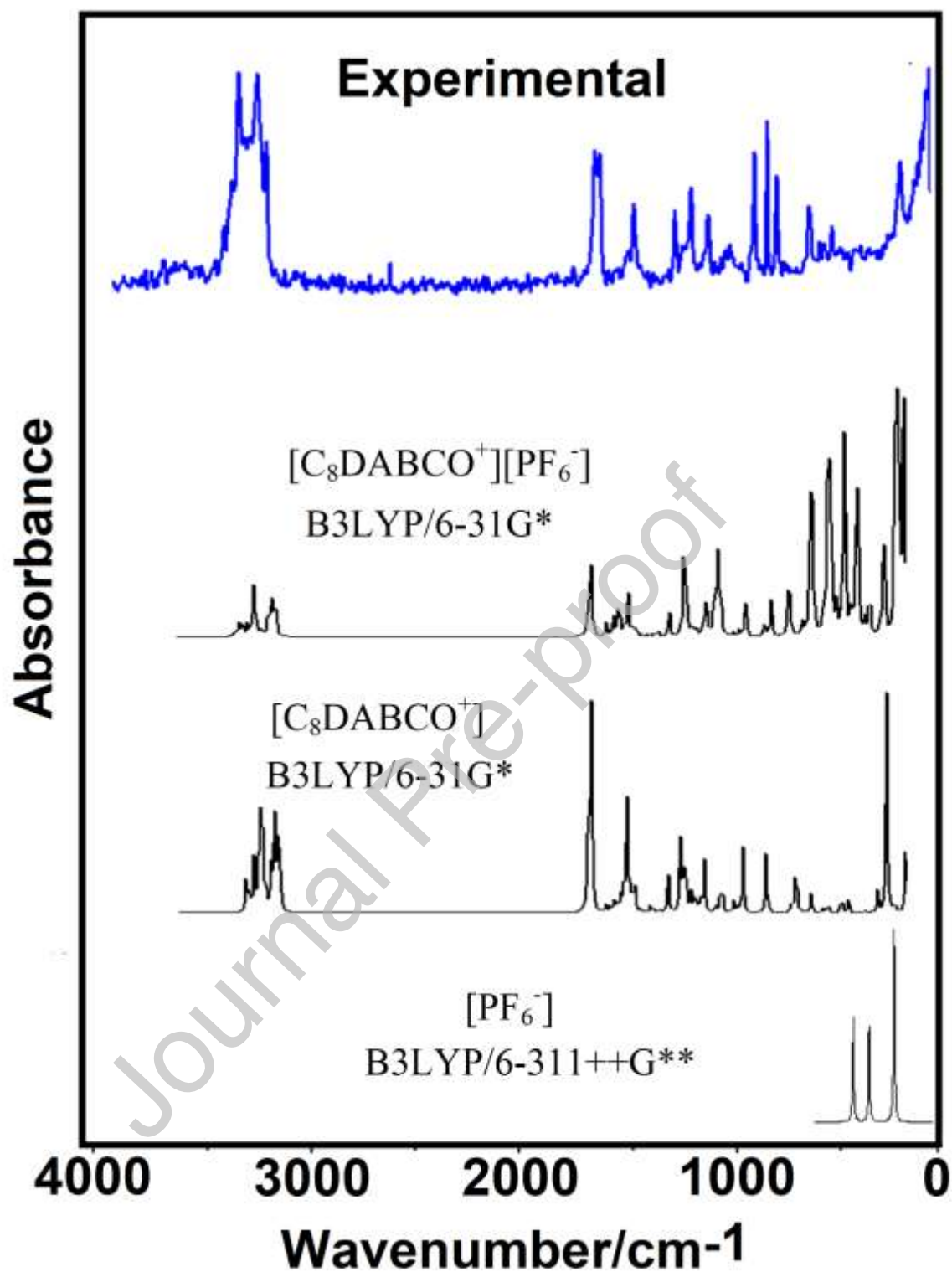


Figure 4. Experimental FT-Raman of $[\text{C}_8\text{DABCO}^+][\text{PF}_6^-]$ IL compared with the corresponding predicted for the cation and anion by using the B3LYP/6-31G* method.

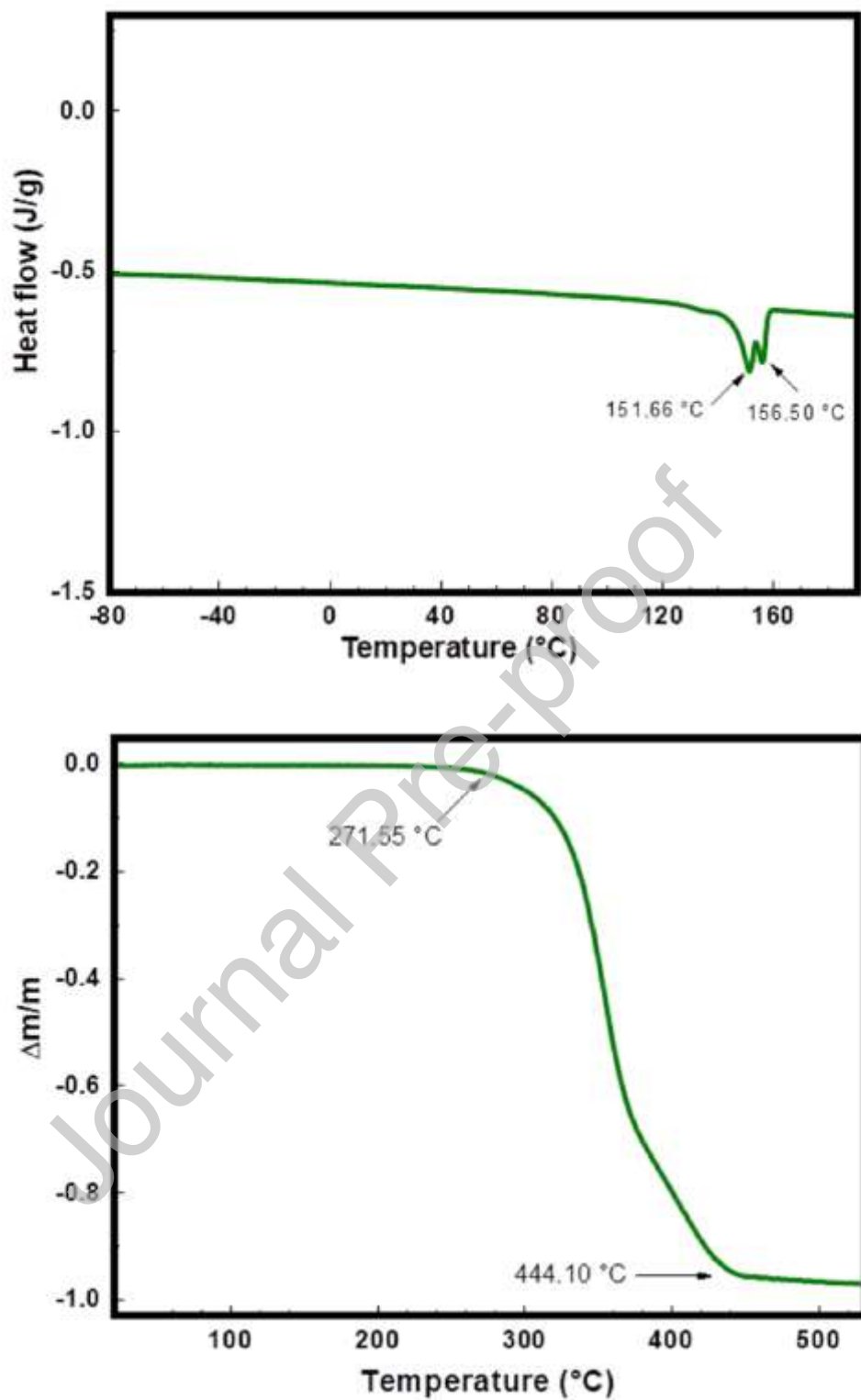


Figure 5. DTA (a) and TGA (b) curves of $[C_8DABCO^+][PF_6^-]$ IL.

Table 1. Calculated total energies (E), dipole moments (μ) and volumes (V) of $[\text{C}_8\text{DABCO}^+][\text{PF}_6^-]$ ionic liquid and its cation and anion in gas phase by using the B3LYP/6-31G* method.

B3LYP/6-31G* Method				
Gas Phase				
Species	E (Hartrees)	E_{ZPVE} (Hartrees)	μ (D)	V (\AA^3)
$[\text{C}_8\text{DABCO}^+][\text{PF}_6^-]$	-1601.3896	-1600.5608	14.39	369.9
$[\text{C}_8\text{DABCO}^+]$	-660.2297	-659.8018	9.90	299.3
$[\text{PF}_6^-]$	-940.6432	-940.6240	0.00	84.5
Aqueous Solution				
$[\text{C}_8\text{DABCO}^+][\text{PF}_6^-]$	-1601.0542	-1600.6056	20.86	377.2

Table 2. Calculated geometrical parameters of $[C_8DABCO^+][PF_6^-]$ ionic liquid in gas phase and aqueous solution and its cation in gas phase by using the B3LYP/6-31G* Method.

B3LYP/6-31G* Method			
$[C_8DABCO^+]^b$		$[C_8DABCO^+][PF_6^-]^a$	
Bond lengths (Å)			
Parameters	Gas	Gas	PCM
N1-C2	1.463	1.468	1.473
N1-C3	1.463	1.464	1.474
N1-C4	1.463	1.470	1.475
N23-C5	1.524	1.527	1.520
N23-C6	1.521	1.510	1.514
N23-C7	1.521	1.525	1.517
C7-H19	1.092	1.088	1.089
C20-H21	1.094	1.090	1.091
RMSD		1.404	1.405
Bond angles (°)			
Parameters	Gas	Gas	PCM
C2-N1-C3	109.5	108.9	108.2
C2-N1-C4	109.5	108.4	107.8
C3-N1-C4	109.6	109.2	108.2
C5-N23-C6	108.2	108.0	107.9
C5-N23-C7	108.1	108.8	108.2
C6-N23-C7	108.6	107.8	108.1
RMSD		0.7	1.1

^aThis work, ^bFrom Ref [15],

Table 3. Observed ^1H chemical shifts (δ in ppm) of $[\text{C}_8\text{DABCO}^+][\text{PF}_6^-]$ IL in CD_3Cl compared with the calculated for the IL in aqueous solution and its cation in gas phase by using the hybrid B3LYP/6-31G* method.

Atoms	$[\text{C}_8\text{DABCO}^+]^{\text{b}}$	$[\text{C}_8\text{DABCO}^+][\text{PF}_6^-]^{\text{a}}$	Exp, ^a
8-H	2.98	2.35	3.15
9-H	2.91	2.88	3.15
10-H	2.89	2.60	3.19
11-H	2.95	2.46	3.19
12-H	2.85	2.49	3.14
13-H	2.97	2.91	3.14
14-H	2.43	2.01	3.22
15-H	2.43	3.86	3.22
16-H	2.25	1.87	3.25
17-H	2.70	2.63	3.25
18-H	2.81	2.14	3.24
19-H	2.18	4.03	3.24
21-H	2.51	4.06	3.12
22-H	2.55	1.88	3.09
25-H	1.31	1.54	1.60
26-H	1.33	0.80	1.57
28-H	1.07	1.65	1.27
29-H	1.08	0.70	1.26
31-H	1.26	1.31	1.24
32-H	1.26	0.97	1.23
34-H	1.20	1.37	1.23
35-H	1.20	1.04	1.21
37-H	1.18	1.01	1.21
38-H	1.18	1.18	1.20
40-H	1.21	1.13	1.20
41-H	1.21	1.27	1.19
43-H	0.99	0.87	0.80
44-H	0.71	0.59	0.81
45-H	0.71	0.68	0.82
RMSD	0.42	0.64	

^aThis work GIAO/B3LYP/6-31G* Ref, to TMS, ^bFrom Ref [7].

Journal Pre-proof

Table 4. Observed ^{13}C chemical shifts (δ in ppm) of $[\text{C}_8\text{DABCO}^+][\text{PF}_6^-]$ IL in CD_3Cl compared with the calculated for the IL in aqueous solution and its cation in gas phase by using the hybrid B3LYP/6-31G* method.

Atoms	$[\text{C}_8\text{DABCO}^+]^{\text{b}}$	$[\text{C}_8\text{DABCO}^+][\text{PF}_6^-]^{\text{a}}$	Experimental ^a
2-C	38.29	55.57	45.05
3-C	38.16	56.18	45.05
4-C	38.16	55.43	45.05
5-C	50.32	64.92	52.65
6-C	44.85	62.07	52.65
7-C	44.69	59.49	52.65
20-C	60.65	74.16	64.99
24-C	17.16	34.49	21.80
27-C	22.23	38.84	26.08
30-C	25.50	43.08	28.90
33-C	25.58	43.13	28.90
36-C	26.87	44.65	31.57
39-C	18.72	36.47	22.48
42-C	8.46	26.47	13.93
RMSD	5.44	11.84	

^aThis work GIAO/B3LYP/6-31G* Ref, to TMS, ^bFrom Ref [7].

Table 5. Observed ^{19}F chemical shifts (δ in ppm) of $[\text{C}_8\text{DABCO}^+][\text{PF}_6^-]$ IL in CD_3Cl compared with the calculated for the IL in aqueous solution and its anion in gas phase by using the hybrid B3LYP/6-31G* method.

Atoms	$[\text{PF}_6^-]^b$	$[\text{C}_8\text{DABCO}^+][\text{PF}_6^-]^a$	Exp ^a
47-F	-62.00	-72.63	-72.62
48-F	-62.00	-81.93	-72.62
49-F	-62.00	-83.03	-71.14
50-F	-62.00	-81.09	-72.62
51-F	-62.00	-73.24	-72.62
52-F	-62.00	-73.17	-72.62
RMSD	6.61	4.37	

^aThis work GIAO/B3LYP/6-31G* Ref, to CCl_3F , ^bFrom Ref [11].

Table 6. Observed and calculated wavenumbers (cm^{-1}) and assignments for $[\text{C}_8\text{DABCO}^+][\text{PF}_6^-]$ ionic liquid and its cation and anion in gas phase by using the hybrid B3LYP Method.

Experimental ^a		B3LYP/6-311++G**			B3LYP/6-31G*				
		[PF ₆ ⁻] ^b		[C ₈ DABCO ⁺] ^c	[C ₈ DABCO ⁺][PF ₆ ⁻] ^a				
IR	Raman	SQM ^b	Assignments	SQM ^c	Assignments	Calc ^d	SQM ^e	Int ^f	Assignments ^g
	3071sh			3046	$\nu_a\text{CH}_2(\text{C}7)$	3212	3051	91.9	$\nu_a\text{CH}_2(\text{C}7)$
				3042	$\nu_a\text{CH}_2(\text{C}6)$	3201	3041	20.3	$\nu_a\text{CH}_2(\text{C}5)$
	3033sh			3031	$\nu_a\text{CH}_2(\text{C}5)$	3175	3016	18.9	$\nu_a\text{CH}_2(\text{C}20)$
				3011	$\nu_a\text{CH}_2(\text{C}20)$	3158	3000	15.9	$\nu_a\text{CH}_2(\text{C}6)$
				3011	$\nu_a\text{CH}_2(\text{C}3)$	3145	2988	12.5	$\nu_a\text{CH}_2(\text{C}4)$
				3009	$\nu_a\text{CH}_2(\text{C}4)$	3129	2973	19.1	$\nu_a\text{CH}_2(\text{C}2)$
	3002sh			3007	$\nu_a\text{CH}_2(\text{C}2)$	3123	2967	22.7	$\nu_a\text{CH}_2(\text{C}24)$
				2992	$\nu_a\text{CH}_3$	3121	2965	2.9	$\nu_s\text{CH}_2(\text{C}3)$
				2982	$\nu_a\text{CH}_3$	3112	2956	41.4	$\nu_s\text{CH}_2(\text{C}7)$
				2981	$\nu_s\text{CH}_2(\text{C}7)$	3113	2957	43.4	$\nu_a\text{CH}_3$
				2980	$\nu_s\text{CH}_2(\text{C}6)$	3106	2951	66.0	$\nu_a\text{CH}_3$
	2974vs			2975	$\nu_a\text{CH}_2(\text{C}24)$	3106	2951	19.0	$\nu_s\text{CH}_2(\text{C}5)$
				2973	$\nu_s\text{CH}_2(\text{C}5)$	3096	2941	7.9	$\nu_s\text{CH}_2(\text{C}6)$
				2969	$\nu_s\text{CH}_2(\text{C}3), \nu_s\text{CH}_2(\text{C}4)$	3085	2931	33.7	$\nu_s\text{CH}_2(\text{C}4)$
				2966	$\nu_s\text{CH}_2(\text{C}3)$	3084	2930	57.2	$\nu_a\text{CH}_2(\text{C}33)$
2964w	2960sh			2965	$\nu_s\text{CH}_2(\text{C}4), \nu_s\text{CH}_2(\text{C}2)$	3079	2925	15.3	$\nu_s\text{CH}_2(\text{C}3)$
				2956	$\nu_s\text{CH}_2(\text{C}20)$	3078	2924	46.4	$\nu_s\text{CH}_2(\text{C}20)$
				2954	$\nu_a\text{CH}_2(\text{C}30), \nu_a\text{CH}_2(\text{C}33)$	3077	2923	17.8	$\nu_s\text{CH}_2(\text{C}2)$
				2943	$\nu_a\text{CH}_2(\text{C}27)$	3072	2918	31.1	$\nu_a\text{CH}_2(\text{C}27)$
				2934	$\nu_s\text{CH}_2(\text{C}24)$	3058	2905	2.9	$\nu_a\text{CH}_2(\text{C}39)$
2929m				2931	$\nu_a\text{CH}_2(\text{C}39)$	3046	2894	11.0	$\nu_a\text{CH}_2(\text{C}33)$
				2921	$\nu_s\text{CH}_3$	3042	2890	45.6	$\nu_s\text{CH}_3$
	2918sh			2920	$\nu_a\text{CH}_2(\text{C}30)$	3037	2885	21.2	$\nu_a\text{CH}_2(\text{C}36)$
				2913	$\nu_a\text{CH}_2(\text{C}36), \nu_a\text{CH}_2(\text{C}33)$	3035	2883	30.9	$\nu_s\text{CH}_2(\text{C}24)$
				2910	$\nu_s\text{CH}_2(\text{C}27)$	3028	2877	69.1	$\nu_s\text{CH}_2(\text{C}39)$
	2904sh			2905	$\nu_s\text{CH}_2(\text{C}39)$	3024	2873	9.9	$\nu_s\text{CH}_2(\text{C}27)$

2885w	2894vs	2899	$\nu_s\text{CH}_2(\text{C30})$	3019	2868	10.4	$\nu_s\text{CH}_2(\text{C30})$
2870w	2880sh	2894	$\nu_s\text{CH}_2(\text{C33})$	3014	2863	3.6	$\nu_s\text{CH}_2(\text{C33})$
2846w	2856s	2891	$\nu_s\text{CH}_2(\text{C36})$	3011	2860	0.7	$\nu_s\text{CH}_2(\text{C36})$
1502w	1514w	1486	$\delta\text{CH}_2(\text{C5})$	1559	1481	11.2	$\delta\text{CH}_2(\text{C7})$
1490sh	1496sh	1476	$\delta\text{CH}_2(\text{C39}), \delta\text{CH}_2(\text{C36})$	1544	1467	6.8	$\delta\text{CH}_2(\text{C39})$
1486sh	1483sh	1472	$\delta_a\text{CH}_3$	1540	1463	5.2	$\delta_a\text{CH}_3$
1477s	1472vs	1468	$\delta\text{CH}_2(\text{C3})$	1536	1459	2.1	$\delta\text{CH}_2(\text{C3})$
1468sh		1465	$\delta_a\text{CH}_3$	1534	1457	10.4	$\delta\text{CH}_2(\text{C2})$
1465sh		1464	$\delta\text{CH}_2(\text{C24})$	1531	1454	4.7	$\delta\text{CH}_2(\text{C6})$
1461sh		1460	$\delta\text{CH}_2(\text{C5}), \delta\text{CH}_2(\text{C6})$	1530	1454	7.3	$\delta_a\text{CH}_3$
1459sh	1453vs	1459	$\delta\text{CH}_2(\text{C7})$	1529	1453	3.8	$\delta\text{CH}_2(\text{C36})$
		1457	$\delta\text{CH}_2(\text{C30}), \delta\text{CH}_2(\text{C39})$	1524	1448	6.4	$\delta\text{CH}_2(\text{C5})$
		1451	$\delta\text{CH}_2(\text{C27}), \delta\text{CH}_2(\text{C39})$	1521	1445	3.8	$\delta\text{CH}_2(\text{C24})$
		1451	$\delta\text{CH}_2(\text{C6}), \delta\text{CH}_2(\text{C2})$	1519	1443	1.11	$\delta\text{CH}_2(\text{C2})$
		1449	$\delta\text{CH}_2(\text{C4})$	1518	1442	0.4	$\delta\text{CH}_2(\text{C27})$
	1439sh	1448	$\delta\text{CH}_2(\text{C33})$	1515	1439	0.9	$\delta\text{CH}_2(\text{C33})$
		1447	$\delta\text{CH}_2(\text{C30}), \delta\text{CH}_2(\text{C36})$	1514	1438	0.2	$\delta\text{CH}_2(\text{C30})$
		1442	$\delta\text{CH}_2(\text{C20})$	1513	1437	0.4	$\delta\text{CH}_2(\text{C20})$
1418w	1413w	1423	wagCH ₂ (C20)	1482	1408	9.1	wagCH ₂ (C20)
1387m	1388sh	1406	wagCH ₂ (C33), wagCH ₂ (C36)	1441	1369	1.3	$\delta_s\text{CH}_3$
1377sh	1371w	1401	wagCH ₂ (C27), wagCH ₂ (C30)	1436	1364	4.5	wagCH ₂ (C7)
		1397	wagCH ₂ (C6)	1427	1356	3.6	$\rho\text{CH}_2(\text{C20})$
	1352sh	1387	wagCH ₂ (C2), wagCH ₂ (C3)	1426	1355	1.7	wagCH ₂ (C33)
1346w	1347sh	1384	$\delta_s\text{CH}_3$	1423	1352	0.4	wagCH ₂ (C36)
1332w	1333sh	1377	$\rho\text{CH}_2(\text{C20}), \text{wagCH}_2(\text{C7})$	1403	1333	2.2	wagCH ₂ (C5)
1332w	1333sh	1374	wagCH ₂ (C27)	1401	1331	9.2	wagCH ₂ (C2)
		1358	wagCH ₂ (C2)	1400	1330	1.3	wagCH ₂ (C4)
	1316sh	1357	wagCH ₂ (C4), wagCH ₂ (C3)	1381	1312	3.2	wagCH ₂ (C3)
1311w	1307s	1349	wagCH ₂ (C5)	1376	1307	2.4	wagCH ₂ (C6)
1311w	1307s	1338	wagCH ₂ (C39)	1369	1301	2.4	wagCH ₂ (C39)
	1298sh	1334	$\rho\text{CH}_2(\text{C3})$	1367	1299	3.2	$\rho\text{CH}_2(\text{C20})$
	1291sh	1330	$\rho\text{CH}_2(\text{C2}), \rho\text{CH}_2(\text{C4})$	1363	1295	3.7	$\rho\text{CH}_2(\text{C24})$

		1325	$\rho\text{CH}_2(\text{C}27)$	1358	1290	1.3	$\rho\text{CH}_2(\text{C}30)$
1287sh		1319	$\rho\text{CH}_2(\text{C}24), \rho\text{CH}_2(\text{C}33)$	1352	1284	0.3	$\rho\text{CH}_2(\text{C}33)$
1287sh		1316	$\rho\text{CH}_2(\text{C}30)$	1352	1284	1.2	$\rho\text{CH}_2(\text{C}36)$
		1311	$\rho\text{CH}_2(\text{C}36)$	1343	1276	1.1	$\rho\text{CH}_2(\text{C}39)$
		1296	$\text{wagCH}_2(\text{C}24)$	1339	1272	1.6	$\rho\text{CH}_2(\text{C}27)$
		1292	$\rho\text{CH}_2(\text{C}39)$	1333	1266	1.2	$\rho\text{CH}_2(\text{C}6)$
1247w		1289	$\rho\text{CH}_2(\text{C}6)$	1318	1252	3.7	$\rho\text{CH}_2(\text{C}5)$
1247w		1263	$\rho\text{CH}_2(\text{C}5)$	1306	1241	1.7	$\text{wagCH}_2(\text{C}30)$
1225w		1242	$\text{wagCH}_2(\text{C}30), \text{wagCH}_2(\text{C}33)$	1286	1222	0.2	$\rho\text{CH}_2(\text{C}7)$
1225w		1241	$\rho\text{CH}_2(\text{C}2), \rho\text{CH}_2(\text{C}4)$	1283	1219	1.0	$\rho\text{CH}_2(\text{C}4)$
1203ww		1221	$\rho\text{CH}_2(\text{C}36), \rho\text{CH}_2(\text{C}24)$	1257	1194	1.6	$\text{wagCH}_2(\text{C}24)$
1180sh		1185	$\rho\text{CH}_2(\text{C}7)$	1241	1179	0.7	$\rho\text{CH}_2(\text{C}3)$
1169sh		1163	$\rho\text{CH}_2(\text{C}30), \rho\text{CH}_2(\text{C}27)$	1230	1169	0.1	$\rho\text{CH}_2(\text{C}2)$
1137sh	1136s	1138	$\nu\text{C}2\text{-N}1$	1224	1163	1.0	$\nu\text{C}3\text{-N}1$
		1130	$\nu\text{C}4\text{-N}1, \nu\text{C}3\text{-N}1$	1216	1155	1.7	$\nu\text{C}2\text{-N}1$
1121sh	1122sh	1122	$\rho\text{CH}_3, \nu\text{C}2\text{-N}1$	1192	1132	1.7	$\tau\text{wCH}_2(\text{C}27)$
1108m	1104m	1089	$\tau\text{wCH}_2(\text{C}27)$	1151	1093	3.2	ρCH_3
1069s	1068s	1074	$\delta\text{C}3\text{C}6\text{N}23, \delta\text{C}6\text{-N}23\text{C}7$	1104	1049	51.6	$\nu\text{C}20\text{-N}23$
1069s	1068s	1067	$\nu\text{C}20\text{-C}24$	1095	1040	11.4	$\nu\text{C}20\text{-C}24$
1069s	1068s	1034	$\nu\text{C}33\text{-C}36, \nu\text{C}36\text{-C}39$	1079	1025	17.6	$\nu\text{C}3\text{-N}1$
1031sh		1027	$\nu\text{C}27\text{-C}30, \nu\text{C}30\text{-C}33$	1077	1023	19.7	$\nu\text{C}4\text{-N}1$
	1020sh	1026	$\nu\text{C}3\text{-N}1, \nu\text{C}4\text{-N}1$	1075	1021	1.6	$\nu\text{C}33\text{-C}36$
1017sh	1011sh	1023	$\nu\text{C}2\text{-N}1$	1071	1017	1.6	$\nu\text{C}24\text{-C}27$
999m	996s	1005	$\nu\text{C}24\text{-C}27, \nu\text{C}39\text{-C}42$	1054	1001	0.4	$\nu\text{C}6\text{-N}23$
999m	996s	998	$\rho\text{CH}_2(\text{C}33)$	1049	997	3.3	$\tau\text{wCH}_2(\text{C}3)$
988sh	981sh	994	$\nu\text{C}27\text{-C}30, \nu\text{C}30\text{-C}33$	1047	995	1.3	$\nu\text{C}30\text{-C}33$
	967w	973	$\nu\text{C}33\text{-C}36, \nu\text{C}5\text{-N}23$	1030	979	3.1	$\nu\text{C}27\text{-C}30$
		958	$\nu\text{C}5\text{-N}23$	1017	966	1.5	$\nu\text{C}5\text{-N}23$
	950sh	956	$\nu\text{C}7\text{-N}23$	1011	960	0.8	$\nu\text{C}7\text{-N}23$
947sh	941sh	948	$\nu\text{C}4\text{-C}7, \nu\text{C}3\text{-C}6$	1001	951	2.2	$\nu\text{C}39\text{-C}42$
927sh	924sh	936	$\tau\text{wCH}_2(\text{C}3), \tau\text{wCH}_2(\text{C}2), \tau\text{wCH}_2(\text{C}5)$	995	945	7.1	$\nu\text{C}4\text{-C}7$
918w		913	$\nu\text{C}4\text{-C}7, \nu\text{C}3\text{-C}6$	971	922	1.7	$\nu\text{C}3\text{-C}6$

900sh	901m		902	vC2-C5	940	893	10.2	vC2-C5	
898sh	894sh		880	ρCH_3	933	886	27.7	$\delta\text{C4C7N23}$	
888m	887sh		877	$\delta\text{C4C7N23}, \delta\text{C3C6N23}$	909	864	261.0	$\nu_a\text{PF}_6(\text{T}_{1u})$	
870sh	852w				908	863	101.9	$\nu\text{C36-C39}$	
833vs	800vs				906	861	206.2	$\nu_a\text{PF}_6(\text{T}_{1u})$	
833vs	800vs				901	856	292.3	$\nu_a\text{PF}_6(\text{T}_{1u})$	
833vs	800vs				901	856	250.9	$\nu_s\text{PF}_6(\text{A}_{1g})$	
833vs	800vs		865	vC20-N23	877	833	11.6	$\tau\text{wCH}_2(\text{C7})$	
			806	$\tau\text{wCH}_2(\text{C36}), \rho'\text{CH}_3$	850	808	14.7	$\tau\text{wCH}_2(\text{C4})$	
			781	vC3-N1, vC4-N1	844	802	6.7	$\tau\text{wCH}_2(\text{C6})$	
797sh	786sh		771	$\tau\text{wCH}_2(\text{C6})$	824	783	3.4	$\tau\text{wCH}_2(\text{C5})$	
772sh	780sh		770	$\tau\text{wCH}_2(\text{C7})$	809	769	3.1	$\tau\text{wCH}_2(\text{C20})$	
747s		797	$\nu_a\text{PF}_6(\text{T}_{1u})$	740	$\tau\text{wCH}_2(\text{C4})$	799	759	12.5	δC4N1C3
734sh	734sh	797	$\nu_a\text{PF}_6(\text{T}_{1u})$	732	$\tau\text{wCH}_2(\text{C39}), \tau\text{wCH}_2(\text{C20})$	767	729	7.6	$\tau\text{wCH}_2(\text{C24})$
713s	706s	797	$\nu_a\text{PF}_6(\text{T}_{1u})$	689	$\tau\text{wCH}_2(\text{C24})$	747	710	2.4	$\tau\text{wCH}_2(\text{C30})$
698sh	694sh		681	vC6-N23	739	702	5.3	$\tau\text{wCH}_2(\text{C33})$	
	676w	652	$\nu_s\text{PF}_6(\text{A}_{1g})$	668	$\tau\text{wCH}_2(\text{C27})$	707	672	44.2	$\nu_s\text{PF}_6(\text{A}_{1g})$
	620w		662	$\tau\text{wCH}_2(\text{C33}), \tau\text{wCH}_2(\text{C30})$	703	668	16.9	$\delta\text{C6N23C20}$	
	594sh		583	$\delta\text{C2C5N23}$	593	563	5.7	$\delta\text{C5N23C20}$	
	572s				574	545	11.4	$\nu_a\text{PF}_6(\text{E}_g)$	
	572s				570	542	1.0	$\delta\text{C4C7N23}$	
	572s	522	$\delta\text{FPF}(\text{T}_{1u})$		567	539	16.3	$\nu_a\text{PF}_6(\text{E}_g)$	
	572s	522	$\delta\text{FPF}(\text{T}_{1u})$	563	$\delta\text{C4C7N23}$	563	535	2.5	$\nu\text{P-F}\cdots\text{H}$
	572s	522	$\delta_s\text{FPF}(\text{T}_{1u})$	554	$\delta\text{C3C6N23}$	529	503	29.8	$\delta\text{FPF}(\text{T}_{1u})$
	572s	511	$\nu_a\text{PF}_6(\text{E}_g)$		528	502	45.1	$\delta\text{FPF}(\text{T}_{1u})$	
495sh	511	$\nu_a\text{PF}_6(\text{E}_g)$			526	500	22.8	$\delta_s\text{FPF}(\text{T}_{1u})$	
473m			497	$\delta\text{C24C27C30}, \delta\text{C33C36C39}$	504	479	2.0	δCCC	
			453	$\delta\text{C36C39C42}$	460	437	1.3	δCCC	
437w	434	$\text{WagFPF}(\text{T}_{2g})$	432	$\delta\text{C5N23C6}, \delta\text{C5N23C7}$	450	428	6.8	$\text{WagFPF}(\text{T}_{2g})$	
	434	$\text{wagFPF}(\text{T}_{2g})$	421	$\delta\text{C6-N23C7}, \delta\text{C4N1C3}$	441	419	0.3	$\text{wagFPF}(\text{T}_{2g})$	
	434	$\text{wagFPF}(\text{T}_{2g})$			441	419	0.2	$\text{wagFPF}(\text{T}_{2g})$	
					437	415	0.3	δCCC	

426sh				429	408	0.2	δ CCC
381w		373	δ C4N1C3, ρ N23-C24	379	360	1.0	δ CCC
351w		364	ρ' N23-C24, δ C4N1C2, δ C3N1C2	376	357	1.4	δ CCC
334sh		338	δ C36C39C42, δ C5N23C7	348	331	0.8	δ CCC
316w		296	δ C6-N23C7	314	298	0.5	δ CCC
				303	288	0.5	δ CCC
	285		ρ FPF(T_{2u})	296	281	0.0	ρ FPF(T_{2u})
277w	285		ρ FPF(T_{2u})	286	272	0.2	ρ FPF(T_{2u})
	285		ρ FPF(T_{2u})	282	268	0.4	ρ FPF(T_{2u})
239w		223	τ wCH ₃	254	241	0.0	τ wCH ₃
214sh		214	ρ N23-C24	219	208	0.8	ρ N23-C20
186vs				177	168	2.6	δ CCC
		166	δ C20C24C27, ν C20-N23	172	163	1.1	τ C-C
148sh		150	τ C33-C30	152	144	0.1	τ C-C
143sh				147	140	2.4	τ C-C
128sh		136	τ C30-C27	136	129	6.0	τ C-C
119sh		116	τ C39-C36	115	109	7.2	τ C-C
111sh		115	δ C33C36C39, δ C30C33C36, δ C24C20N23	106	101	7.7	τ C-C
99sh		84	τ C36-C33	91	86	1.0	τ C-C
78sh				78	74	2.8	ν P-F...H
78sh				73	69	0.9	τ wC20-N23
66vs		69	τ C36-C33, τ C24-C20	67	64	0.8	τ wP-F...H
		58	τ wC20-N23	58	55	0.4	τ wPF ₆ ⁻
				47	45	0.6	τ C-C
		43	δ C24C27C30, δ C27C30C33, δ C20C24C27	42	40	0.6	τ C-C
		35	τ wC20-N23, τ C24-C20	31	29	0.1	τ C-C
		26	τ C24-C20, τ C27-C24	22	21	0.2	τ C-C
				13	12	3.2	τ C-C

Abbreviations: ν , stretching; δ , deformation in the plane; γ , deformation out of plane; wag, wagging; τ , torsion; ρ , rocking; τ w, twisting; δ , deformation; a, antisymmetric; s, symmetric; ^aThis work, ^bFrom Ref [18] scaled quantum mechanics force field with B3LYP/6-311++G** method, ^cFrom Ref [15] scaled quantum mechanics force field with B3LYP/6-31G* method; ^dFrom B3LYP/6-31G* method, ^eFrom scaling factor 0.95; ^fIntensities in KM/Mole.